The current issue and full text archive of this journal is available at
www.emeraldinsight.com/0961-5539.htm

Meshless local radial basis function collocation method for convective-diffusive solid-liquid phase change problems

Robert Vertnik and Božidar Šarler
Laboratory for Multiphase Processes, Nova Gorica Polytechnic, Nova Gorica, Slovenia

Received April 2005
Revised August 2005
Accepted November 2005

Abstract

Purpose – The purpose of this paper is to develop a new local radial basis function collocation method (LRBFCM) for one-domain solving of the non-linear convection-diffusion equation, as it appears in mixture continuum formulation of the energy transport in solid-liquid phase change systems.

Design/methodology/approach – The method is structured on multiquadrics radial basis functions. The collocation is made locally over a set of overlapping domains of influence and the time stepping is performed in an explicit way. Only small systems of linear equations with the dimension of the number of nodes in the domain of influence have to be solved for each node. The method does not require polygonisation (meshing). The solution is found only on a set of nodes.

Findings – The computational effort grows roughly linearly with the number of the nodes. Results are compared with the existing steady analytical solutions for one-dimensional convective-diffusive problem with and without phase change. Regular and randomly displaced node arrangements have been employed. The solution is compared with the results of the classical finite volume method. Excellent agreement with analytical solution and reference numerical method has been found.

Practical implications – A realistic two-dimensional non-linear industrial test associated with direct-chill, continuously cast aluminium alloy slab is presented.

Originality/value – A new meshless method is presented which is simple, efficient, accurate, and applicable in industrial convective-diffusive solid-liquid phase-change problems with non-linear material properties.

Keywords Convection, Diffusion, Meshes, Solids, Liquids

Paper type Research paper

1. Introduction

The problems in science and engineering are usually reduced to a set of coupled partial differential equations (PDEs). It is not easy to obtain their analytical solution, particularly in non-linear and complex-shaped cases, and discrete approximate methods have to be employed accordingly. The finite difference method (FDM) (Özisik, 1994), the finite volume method (FVM) (Versteeg and Malalasekera, 1995), the finite element method (FEM) (Zienkiewicz and Taylor, 2000), and the boundary element

The authors would like to acknowledge the aluminium enterprise IMPOL Slovenska Bistrica, Slovenia, and the Slovenian Ministry of High Education, Science and Technology for support in the framework of the project Modeling and optimization for competitive continuous casting.

International Journal of Numerical Methods for Heat & Fluid Flow
Vol. 16 No. 5, 2006
pp. 617-640

0961-5539
DOI 10.1108/09615530610669148

method (BEM) (Wrobel, 2001) are the most widely used among them at the present. Despite the powerful features of these methods, there are often substantial difficulties in applying them to realistic, geometrically complex three-dimensional transient situations with moving and/or deforming boundaries. A common complication in the mentioned methods is the need to create a polygonisation, either in the domain and/or on its boundary. This type of (re)meshing is often the most time consuming part of the solution process and is far from being fully automated. In the recent years, a new class of methods is in development, which do not require polygonisation but use only a set of nodes to approximate the solution. The rapid development of these types of mesh-free (meshless, polygon-free) methods and their classification is elaborated in the very recent monographs (Atluri and Shen, 2002; Liu, 2003; Atluri, 2004; Šarler, 2004). A broad class of mesh-free methods in development today are based on radial basis functions (RBFs) (Buhmann, 2003). The RBF collocation method (RBFCM) or Kansa (1990) method is the simplest of them. It is based on the strong formulation of the governing PDE. This method has been further upgraded to symmetric collocation (Fasshauer, 1997), (Power and Barraco, 2002), to modified collocation (Chen, 2002) and to indirect collocation (Mai-Duy and Tran-Cong, 2003). The method has been already used in a broad spectrum of computational fluid dynamics problems (Šarler, 2005) such as the solution of Navier-Stokes equations (Mai-Duy and Tran-Cong, 2003) or porous media flow (Šarler *et al.*, 2004) and the solution of solid-liquid phase change problems (Kovačević *et al.*, 2003). In contrast to advantages over mesh generation, all the listed methods unfortunately fail to perform for large problems, because they produce fully populated matrices, sensitive to the choice of the free parameters in RBFs. One of the possibilities for mitigating this problem is to employ the domain decomposition (Mai-Duy and Tran-Cong, 2002). However, the domain decomposition re-introduces some sort of meshing which is not attractive. The concept of local collocation has been in the context of RBF-based solution of Poisson equation introduced by Lee *et al.* (2003). The authors use for interpolation of the function value in a certain node only data in the (neighbouring) nodes that fall into domain of influence of this node. The procedure results in a matrix that is of the same size as the matrix in the original Kansa method, however it is sparse. The differential quadrature method, that calculates the derivatives of a function by a weighted linear sum of functional values at its neighbouring nodes has been structured with the RBFs by Shu *et al.* (2003). Despite the local properties, the matrix still has a similar form as in Lee *et al.* (2003). A parallel development, based on strong formulation, polynomials instead of RBF and least squares approximation instead of collocation is in development under name diffuse approximate method (Nayroles *et al.*, 1991; Sadat and Prax, 1996; Vertnik *et al.*, 2004; Šarler *et al.*, 2005; Perko, 2005).

In this paper, the local radial basis function collocation method (LRBFCM) is developed to solve non-linear convective-diffusive transport phenomena problems with non-linear material properties and phase change, and applied to the one-dimensional test cases and two-dimensional industrial continuous casting problem. The developments are based on our experience (Šarler and Vertnik, 2005) in related solving of the diffusion equation.

2. Governing equations

Consider a connected fixed domain Ω with boundary Γ occupied by a liquid-solid phase change material described with the temperature dependent density ρ_φ of the phase φ temperature dependent specific heat at constant pressure c_φ, thermal conductivity k_φ, and the specific latent heat of the solid-liquid phase change h_m. The mixture continuum formulation (Bennon and Incropera, 1987) of the enthalpy conservation for the assumed system is:

$$\frac{\partial}{\partial t}(\rho h) + \nabla\cdot(\rho\vec{v}h) = \nabla\cdot(k\nabla T) + \nabla\cdot\left(\rho\vec{v}h - f_{\mathrm{S}}^{\mathrm{V}}\rho_{\mathrm{S}}\vec{v}_{\mathrm{S}}h_{\mathrm{S}} - f_{\mathrm{L}}^{\mathrm{V}}\rho_{\mathrm{L}}\vec{v}_{\mathrm{L}}h_{\mathrm{L}}\right) \tag{1}$$

with mixture density and thermal conductivity defined as:

$$\rho = f_{\mathrm{S}}^{\mathrm{V}}\rho_{\mathrm{S}} + f_{\mathrm{L}}^{\mathrm{V}}\rho_{\mathrm{L}} \tag{2}$$

$$k = f_{\mathrm{S}}^{\mathrm{V}}k_{\mathrm{S}} + f_{\mathrm{L}}^{\mathrm{V}}k_{\mathrm{L}} \tag{3}$$

where f_φ^{V} represents the volume fraction of the phase φ. The liquid volume fraction $f_{\mathrm{L}}^{\mathrm{V}}$ is assumed to vary from 0 to 1 between solidus T_{S} and liquidus temperature T_{L}. Mixture velocity is defined as:

$$\vec{v} = \frac{\left(f_{\mathrm{S}}^{\mathrm{V}}\rho_{\mathrm{S}}\vec{v}_{\mathrm{S}} + f_{\mathrm{L}}^{\mathrm{V}}\rho_{\mathrm{L}}\vec{v}_{\mathrm{L}}\right)}{\rho} \tag{4}$$

and mixture enthalpy is defined as:

$$h = f_{\mathrm{S}}^{\mathrm{V}}h_{\mathrm{S}} + f_{\mathrm{L}}^{\mathrm{V}}h_{\mathrm{L}} \tag{5}$$

The constitutive temperature-enthalpy relationships are:

$$h_{\mathrm{S}} = \int_{T_{\mathrm{ref}}}^{T} c_{\mathrm{S}}\,\mathrm{d}T \tag{6}$$

$$h_{\mathrm{L}} = h_{\mathrm{S}}(T) + \int_{T_{\mathrm{S}}}^{T}(c_{\mathrm{L}} - c_{\mathrm{S}})\,\mathrm{d}T + h_m \tag{7}$$

with T_{ref} standing for the reference temperature. Thermal conductivity and specific heat of the phases can arbitrarily depend on temperature. We seek for mixture temperature at time $t_0 + \Delta t$ by assuming known initial temperature, velocity field, and boundary conditions at time t_0. The initial value of the temperature $T(\mathbf{p},t)$ at a point with position vector $\mathbf{p}$ and time t_0 is defined through the known function T_0:

$$T(\mathbf{p},t) = T_0(\mathbf{p});\ \ \mathbf{p}\in\Omega+\Gamma \tag{8}$$

The boundary Γ is divided into not necessarily connected parts $\Gamma = \Gamma^{\mathrm{D}}\cup\Gamma^{\mathrm{N}}\cup\Gamma^{\mathrm{R}}$ with Dirichlet, Neumann and Robin type boundary conditions, respectively. At the boundary point $\mathbf{p}$ with normal $\mathbf{n}_\Gamma$ and time $t_0 \le t \le t_0 + \Delta t$, these boundary conditions are defined through known functions T_Γ^{D}, T_Γ^{N}, T_Γ^{R}, $T_{\Gamma\mathrm{ref}}^{\mathrm{R}}$:

$$T = T_{\Gamma}^{\mathrm{D}};\ \ \mathbf{p} \in \Gamma^{\mathrm{D}} \tag{9}$$

$$\frac{\partial}{\partial n_{\Gamma}} T = T_{\Gamma}^{\mathrm{N}};\ \ \mathbf{p} \in \Gamma^{\mathrm{N}} \tag{10}$$

$$\frac{\partial}{\partial n_{\Gamma}} T = T_{\Gamma}^{\mathrm{R}}\left(T - T_{\Gamma\mathrm{ref}}^{\mathrm{R}}\right);\quad \mathbf{p} \in \Gamma^{\mathrm{R}} \tag{11}$$

3. Solution procedure

3.1 Meshless representation of temperature and its spatial derivatives

The representation of temperature over a set of ${}_{l}N$ (in general) non-equally spaced nodes ${}_{l}\mathbf{p}_{n};\ \ n = 1, 2, \ldots, {}_{l}N$ is made in the following way:

$$T(\mathbf{p}) \approx \sum_{k=1}^{{}_{l}K} {}_{l}\psi_{k}(\mathbf{p})_{l}\alpha_{k} \tag{12}$$

where ${}_{l}\psi_{k}$ stands for the shape functions, ${}_{l}\alpha_{k}$ for the coefficients of the shape functions, and ${}_{l}K$ represents the number of the shape functions. The left lower index on entries of expression (12) represents the domain of influence (subdomain) ${}_{l}\boldsymbol{\omega}$ on which the coefficients ${}_{l}\alpha_{k}$ are determined. The domains of influence ${}_{l}\boldsymbol{\omega}$ can in general be contiguous (overlapping) or non-contiguous (non-overlapping). Each of the domains of influence ${}_{l}\boldsymbol{\omega}$ includes ${}_{l}N$ nodes of which ${}_{l}N_{\Omega}$ can in general be in the domain and ${}_{l}N_{\Gamma}$ on the boundary, i.e. ${}_{l}N = {}_{l}N_{\Omega} + {}_{l}N_{\Gamma}$. The total number of all nodes $\mathbf{p}_{n}$ is equal $N = N_{\Omega} + N_{\Gamma}$ of which N_{Γ} are located on the boundary and N_{Ω} are located in the domain. The domain of influence of the node ${}_{l}\mathbf{p}$ is defined with the nodes having the nearest ${}_{l}N - 1$ distances to the node ${}_{l}\mathbf{p}$. The five nodded ${}_{l}N = 5$ and seven nodded supports ${}_{l}N = 7$ are used in this paper. The coefficients can be calculated from the subdomain nodes at least in two distinct ways. The first way is collocation (interpolation) and the second way is approximation by the least squares method. Only the simpler collocation version for calculation of the coefficients is considered in this text. Let us assume the known function values ${}_{l}T_{n}$ in the nodes ${}_{l}\mathbf{p}_{n}$ of the subdomain ${}_{l}\boldsymbol{\omega}$. The collocation implies:

$$T({}_{l}\mathbf{p}_{n}) = \sum_{k=1}^{{}_{l}N} {}_{l}\psi_{k}({}_{l}\mathbf{p}_{n})_{l}\alpha_{k} \tag{13}$$

For the coefficients to be computable, the number of the shape functions has to match the number of the collocation points ${}_{l}K = {}_{l}N$, and the collocation matrix has to be non-singular. The system of equations (13) can be written in a matrix-vector notation:

$${}_{l}\underline{\psi}_{l}\alpha = {}_{l}\mathbf{T};\ \ {}_{l}\underline{\psi}_{kn} = {}_{l}\psi_{k}({}_{l}\mathbf{p}_{n}),_{l}T_{n} = T({}_{l}\mathbf{p}_{n}) \tag{14}$$

The coefficients ${}_{l}\boldsymbol{\alpha}$ can be computed by inverting the system (14):

$${}_{l}\alpha = {}_{l}\underline{\psi}_{l}^{-1}\mathbf{T} \tag{15}$$

By taking into account the expressions for the calculation of the coefficients ${}_l\alpha$, the collocation representation of temperature $T(\mathbf{p})$ on subdomain ${}_l\omega$ can be expressed as:

$$T(\mathbf{p}) \approx \sum_{k=1}^{{}_lN} {}_l\psi_k(\mathbf{p}) \sum_{n=1}^{{}_lN} \underline{\psi}^{-1}_{kn\ l} T_n. \tag{16}$$

Let us introduce a two dimensional Cartesian coordinate system with base vectors $\mathbf{i}_\varsigma$; $\varsigma = x, y$ and coordinates p_ς; $\varsigma = x, y,$, i.e. $\mathbf{p} = \mathbf{i}_x p_x + \mathbf{i}_y p_y$. The first partial spatial derivatives of $\underline{T}(\mathbf{p})$ on subdomain ${}_l\omega$ can be expressed as:

$$\frac{\partial}{\partial p_\varsigma} T(\mathbf{p}) \approx \sum_{k=1}^{{}_lN} \frac{\partial}{\partial p_\varsigma} {}_l\psi_k(\mathbf{p}) \sum_{n=1}^{{}_lN} {}_l\underline{\psi}^{-1}_{kn\ l} T_n; \quad \varsigma = x, y \tag{17}$$

The second partial spatial derivatives of $T(\mathbf{p})$ on subdomain ${}_l\omega$ can be expressed as:

$$\frac{\partial^2}{\partial p_\varsigma p_\xi} T(\mathbf{p}) \approx \sum_{k=1}^{{}_lN} \frac{\partial^2}{\partial p_\varsigma p_\xi} {}_l\psi_k(\mathbf{p}) \sum_{n=1}^{{}_lN} {}_l\underline{\psi}^{-1}_{kn\ l} T_n; \quad \varsigma, \xi = x, y \tag{18}$$

The RBFs, such as multiquadrics, can be used for the shape functions:

$${}_l\psi_k(\mathbf{p}) = \left[{}_lr_k^2(\mathbf{p}) + c^2\, {}_lr_0^2 \right]^{1/2}; \quad {}_lr_k^2 = (\mathbf{p} -_l \mathbf{p}_k) \cdot (\mathbf{p} -_l \mathbf{p}_k) \tag{19}$$

where c represents the dimensionless shape parameter. The scaling parameter ${}_lr_0^2$ is set to the maximum nodal distance in the domain of influence:

$${}_lr_0^2 = \max {}_lr_m^2({}_l\mathbf{p}_n); \quad m, n = 1, 2, \ldots, {}_lN \tag{20}$$

The explicit values of the involved first and second derivatives of $\psi_k(\mathbf{p})$ are:

$$\frac{\partial}{\partial p_x} {}_l\psi_k(\mathbf{p}) = \frac{p_x -_l p_{kx}}{\left({}_lr_k^2 + c^2\, {}_lr_0^2 \right)^{1/2}} \tag{21}$$

$$\frac{\partial}{\partial p_y} {}_l\psi_k(\mathbf{p}) = \frac{p_y -_l p_{ky}}{\left({}_lr_k^2 + c^2\, {}_lr_0^2 \right)^{1/2}} \tag{22}$$

$$\frac{\partial^2}{\partial p_x^2} {}_l\psi_k(\mathbf{p}) = \frac{(p_y -_l p_{ky})^2 + c^2\, {}_lr_0^2}{\left({}_lr_k^2 + c^2\, {}_lr_0^2 \right)^{3/2}} \tag{23}$$

$$\frac{\partial^2}{\partial p_y^2} {}_l\psi_k(\mathbf{p}) = \frac{(p_x -_l p_{kx})^2 + c^2\, {}_lr_0^2}{\left({}_lr_k^2 + c^2\, {}_lr_0^2 \right)^{3/2}} \tag{24}$$

$$\frac{\partial^2}{\partial p_x p_y}{}_l\psi_k(\mathbf{p}) = \frac{\partial^2}{\partial p_y p_x}{}_l\psi_k(\mathbf{p}) = -\frac{(p_x - {}_l p_{kx})(p_y - {}_l p_{ky})}{\left({}_l r_k^2 + c^2\,{}_l r_0^2\right)^{3/2}} \tag{25}$$

3.2 Meshless solution of the convection-diffusion equation

What follows elaborates the solution of the convection-diffusion equation (1), subject to the initial condition (8), and the boundary conditions (9)-(11). The temperature can be iteratively expressed from the enthalpy as:

$$h = \underline{h} + \frac{\mathrm{d}h}{\mathrm{d}T}(\underline{T})(T - \underline{T}) \tag{26}$$

where $\underline{h}$ represents the known value from previous iteration. The convection-diffusion equation can be transformed into the following expression by taking into account the explicit time discretization and iterative enthalpy-temperature relationship:

$$\begin{aligned}\frac{\partial(\rho h)}{\partial t} &\approx \frac{\rho_0 c_0 h - \rho_0 c_0 h_0}{\Delta t} = \frac{\rho_0 c_0\left[\underline{h} + \frac{\mathrm{d}h}{\mathrm{d}T}(T - \underline{T})\right] - \rho_0 c_0 h_0}{\Delta t} \\ &= -\nabla\cdot(c_0 v_0 h_0) + \nabla\cdot(k_0 \nabla T_0)\end{aligned} \tag{27}$$

The unknown function value T_l in domain node $\mathbf{p}_l$ can be calculated as:

$$T_l = \frac{\left\{h_{0l} + \frac{\mathrm{d}h}{\mathrm{d}T_l}\underline{T}_l - \underline{h}_l + \frac{\Delta t}{\rho_{0l} c_{0l}}[-\nabla\cdot(c_{0l} v_{0l} h_{0l}) + \nabla k_{0l}\cdot\nabla T_{0l} + k_{0l}\cdot\nabla^2 T_{0l}]\right\}}{(\mathrm{d}h/\mathrm{d}T_l)} \tag{28}$$

The handling of the governing equation belongs to the class of fixed-grid or one-domain techniques for phase change problems (Voller *et al.*, 1990). The explicit calculation of expression (28) in 2D is:

$$\begin{aligned}T_l = \Bigg\{ & h_{0l} + \frac{\mathrm{d}h}{\mathrm{d}T_l}\underline{T}_l - \underline{h}_l + \frac{\Delta t}{\rho_{0l} c_{0l}}\left[\sum_{k=1}^{{}_lN}\frac{\partial}{\partial p_{xl}}\psi_k(\mathbf{p}_l)\sum_{n=1}^{{}_lN}{}_l\underline{\psi}^{-1}_{kn\,l}(c_0 v_{0x} h_0)_n\right. \\ & \left. + \sum_{k=1}^{{}_lN}\frac{\partial}{\partial p_y}{}_l\psi_k(\mathbf{p}_l)\sum_{n=1}^{{}_lN}{}_l\underline{\psi}^{-1}_{kn\,l}(c_0 v_{0x} h_0)n\right] \\ & + \frac{\Delta t}{\rho_{0l} c_{0l}}\left[\sum_{k=1}^{{}_lN}\frac{\partial}{\partial p_x}{}_l\psi_k(\mathbf{p}_l)\sum_{n=1}^{{}_lN}{}_l\underline{\psi}^{-1}_{kn\,l}K_{0n}\right]\cdot\left[\sum_{k=1}^{{}_lN}\frac{\partial}{\partial p_x}{}_l\psi_k(\mathbf{p}_l)\sum_{n=1}^{{}_lN}{}_l\underline{\psi}^{-1}_{kn\,l}T_{0n}\right] \\ & + \frac{\Delta t}{\rho_{0l} c_{0l}}\left[\sum_{k=1}^{{}_lN}\frac{\partial}{\partial p_y}{}_l\psi_k(\mathbf{p}_l)\sum_{n=1}^{{}_lN}{}_l\underline{\psi}^{-1}_{kn\,l}K_{0n}\right]\cdot\left[\sum_{k=1}^{{}_lN}\frac{\partial}{\partial p_y}{}_l\psi_k(\mathbf{p}_l)\sum_{n=1}^{{}_lN}{}_l\underline{\psi}^{-1}_{kn\,l}T_{0n}\right] \\ & + \frac{\Delta t k_{0l}}{\rho_{0l} c_{0l}}\left[\sum_{n=1}^{{}_lN}\frac{\partial^2}{\partial p_x^2}{}_l\psi_k(\mathbf{p}_l)\sum_{n=1}^{{}_lN}{}_l\underline{\psi}^{-1}_{kn\,l}T_{0n} + \sum_{n=1}^{{}_lN}\frac{\partial^2}{\partial p_y^2}{}_l\psi_k(\mathbf{p}_l)\sum_{n=1}^{{}_lN}{}_l\underline{\psi}^{-1}_{kn\,l}T_{0n}\right]\Bigg\}\Bigg/\frac{\mathrm{d}h}{\mathrm{d}T_l}\end{aligned} \tag{29}$$

where the formulas (17) and (18) have been employed. The complete solution procedure follows the below defined steps 1-4.

(1) First, the initial conditions are set in the domain and boundary nodes and the required derivatives are calculated from the known nodal values.

(2) The equation (29) is used to calculate the new values of the variable ${}_lT_n$ at time $t_0 + \Delta t$ in the domain nodes.

(3) What follows in the steps 3 and 4 defines variable ${}_lT_n$ at time $t_0 + \Delta t$ in the Dirichlet, Neumann, and Robin boundary nodes. For this purpose, in the step 3, the coefficients ${}_l\alpha$ have to be determined from the new values in the domain and from the information on the boundary conditions. Let us introduce domain, Dirichlet, Neumann, and Robin boundary indicators for this purpose. These indicators are defined as:

$$\Upsilon_{\Omega n} = \begin{cases} 1; \mathbf{p}_n \in \Omega \\ 0; \mathbf{p}_n \notin \Omega \end{cases}, \quad \Upsilon^{\mathrm{D}}_{\Gamma n} = \begin{cases} 1; \mathbf{p}_n \in \Gamma^{\mathrm{D}} \\ 0; \mathbf{p}_n \notin \Gamma^{\mathrm{D}} \end{cases},$$
$$\Upsilon^{N}_{\Gamma n} = \begin{cases} 1; \mathbf{p}_n \in \Gamma^{\mathrm{N}} \\ 0; \mathbf{p}_n \notin \Gamma^{\mathrm{N}} \end{cases}, \quad \Upsilon^{\mathrm{R}}_{\Gamma n} = \begin{cases} 1; \mathbf{p}_n \in \Gamma^{\mathrm{R}} \\ 0; \mathbf{p}_n \notin \Gamma^{\mathrm{R}} \end{cases} \tag{30}$$

The coefficients ${}_l\alpha$ are calculated from the system of linear equations:

$$\sum_{k=1}^{{}_lN} {}_l\Upsilon_{\Omega n\,l}\psi_k({}_l\mathbf{p}_n){}_l\alpha_k + \sum_{k=1}^{{}_lN} {}_l\Upsilon^{\mathrm{D}}_{\Gamma n\,l}\psi_k({}_l\mathbf{p}_n){}_l\alpha_k + \sum_{k=1}^{{}_lN} {}_l\Upsilon^{N}_{\Gamma n} \frac{\partial}{\partial n_\Gamma} {}_l\psi_k({}_l\mathbf{p}_n){}_l\alpha_k$$
$$+ \sum_{k=1}^{{}_lN} {}_l\Upsilon^{\mathrm{R}}_{\Gamma n} \frac{\partial}{\partial n_\Gamma} {}_l\psi_k({}_l\mathbf{p}_n){}_l\alpha_k = {}_l\Upsilon_{\Omega n\,l}T_n + {}_l\Upsilon^{\mathrm{D}}_{\Gamma n\,l}T^{\mathrm{D}}_n + {}_l\Upsilon^{N}_{\Gamma n\,l}T^{N}_n \tag{31}$$
$$+ {}_l\Upsilon^{\mathrm{R}}_{\Gamma n\,l}T^{\mathrm{R}}_{\Gamma n}\left(\sum_{k=1}^{{}_lN} {}_l\psi_k({}_l\mathbf{p}_n){}_l\alpha_k - {}_lT^{\mathrm{R}}_{\Gamma \mathrm{ref}\,n}\right)$$

The system (31) can be written in a compact form:

$${}_l\underline{\Psi}_l\alpha = {}_l\mathbf{b} \tag{32}$$

with the following system matrix entries:

$${}_l\underline{\Psi}_{nk} = {}_l\Upsilon_{\Omega n\,l}\psi_k({}_l\mathbf{p}_n) + {}_l\Upsilon^{\mathrm{D}}_{\Gamma n\,l}\psi_k({}_l\mathbf{p}_n)$$
$$+ {}_l\Upsilon^{N}_{\Gamma n} \frac{\partial}{\partial n_\Gamma} {}_l\psi_k({}_l\mathbf{p}_n) + {}_l\Upsilon^{\mathrm{R}}_{\Gamma n}\left[\frac{\partial}{\partial n_\Gamma} {}_l\psi_k({}_l\mathbf{p}_n) - {}_lT^{\mathrm{R}}_{\Gamma n}\sum_{k=1}^{{}_lN} {}_l\psi_k({}_l\mathbf{p}_n)\right] \tag{33}$$

and with the following explicit form of the augmented right hand side vector:

$${}_l\mathbf{b}_n = {}_l\Upsilon_{\Omega n}T_n + {}_l\Upsilon^{\mathrm{D}}_{\Gamma n}T^{\mathrm{D}}_{\Gamma n} + {}_l\Upsilon^{N}_{\Gamma n}T^{N}_{\Gamma n} - {}_l\Upsilon^{\mathrm{R}}_{\Gamma n l}T^{\mathrm{R}}_{\Gamma n l}T^{\mathrm{R}}_{\Gamma \mathrm{ref}\,n} \tag{34}$$

(4) The unknown boundary values are set from equation (13).

The under-relaxation might be required in the general case for all the computational nodes:

$$\mathbf{p}_n;\ \ n = 1, 2, \ldots, N \quad T_n = \underline{T}_n + \varepsilon(T_n - \underline{T}_n) \tag{35}$$

with ε standing for the under-relaxation factor. The iterations over one time-step are completed when the iteration criterion:

$$\max|T_n - T_{0n}| \leq T_{\text{itr}} \tag{36}$$

is satisfied in all computational nodes. The steady-state is achieved when the criterion:

$$\max|T_n - T_{0n}| \leq T_{\text{ste}} \tag{37}$$

is met. The parameter T_{ste} is defined as the steady-state convergence margin. In case the steady-state criterion is achieved or the time of calculation exceeds the foreseen time of interest, the calculation is stopped.

4. Numerical examples

4.1 Convective-diffusive problem with different material properties of the phases

To the best of the authors' knowledge, the exact closed form solution for checking convective-diffusive solid-liquid phase change problems appears to exist only for a relatively simple one-dimensional steady-state class of problems with uniform velocity field. The solution used by Pardo and Weckman (1986) for checking their one-domain FEM-based numerical method belongs to this class of problems. Pardo and Weckman's solution for equal and constant thermal properties of the phases has been generalized by Šarler and Kuhn (1998) to cope with the generally different and constant thermal properties of the solid $k_{0\text{S}}$, $c_{0\text{S}}$ and liquid $k_{0\text{L}}$, $c_{0\text{L}}$ phase. The extended analytical solution is particularly useful because it allows one to check the proper response of the numerical method regarding the temperature dependence of the material properties. The respective test case is defined as follows: The domain Ω is described by the Cartesian coordinates $p_x^- < p_x < p_x^+$ and $p_y^- < p_y < p_y^+$. Because the one-dimensional problem is solved in two dimensions, the transversal length $p_y^+ - p_y^-$ becomes a free parameter. The boundary conditions at p_x^- and at p_x^+ are of the Dirichlet type with uniform temperatures $T_\Gamma = T_\Gamma^-$ and $T_\Gamma = T_\Gamma^+$. Thermal insulation boundary conditions of the Neumann type are assumed at the boundaries p_y^- and p_y^+. The material moves with the constant uniform velocity $\mathbf{v} = \mathbf{v}_{\text{S}} = \mathbf{v}_{\text{L}}$ with components $v_x = v_0$ and $v_y = 0\,\text{m/s}$. The boundary temperatures and the isothermal melting temperature are related by $T_{\Gamma^-} > T_M > T_{\Gamma^+}$. The liquid phase thus occupies the domain between p_x^- and the interphase boundary at p_{Mx}, and the solid phase the domain between p_{Mx} and p_x^+. The corresponding exact temperature distribution in phase $\wp$ has been found (Šarler and Kuhn 1998) to be:

$$T^P(p_x, p_y) = -\frac{\alpha_P}{v_x} \exp\left(\frac{v_x}{\alpha_P} p_x + A_P\right) + B_P \tag{38}$$

$$\alpha_P = \frac{k_{0P}}{\rho_0 c_{p0P}}; \quad \wp = \text{S}, \text{L} \tag{39}$$

with α_P denoting the thermal diffusivity of the phase $\wp$; the four constants are:

$$A_{\mathrm{S}} = \log \frac{\frac{v_x}{\alpha_{\mathrm{S}}}(T_M - T_{\Gamma^+})}{\exp\left(\frac{v_x}{\alpha_{\mathrm{S}}} p_x^+\right) - \exp\left(\frac{v_x}{\alpha_{\mathrm{S}}} p_{Mx}\right)}, \tag{40}$$

$$A_{\mathrm{L}} = \log \frac{\frac{v_x}{\alpha_{\mathrm{L}}}(T_M - T_{\Gamma^-})}{\exp\left(\frac{v_x}{\alpha_{\mathrm{L}}} p_x^-\right) - \exp\left(\frac{v_x}{\alpha_{\mathrm{L}}} p_{Mx}\right)}, \tag{41}$$

$$B_P = T_M + \frac{\alpha_P}{v_x} A_P \exp\left(\frac{v_x}{\alpha_P} p_{Mx}\right); \quad \wp = \mathrm{S}, \mathrm{L} \tag{42}$$

The position of the interphase boundary is determined from the transcendental equation:

$$-\rho_0 h_M v_x = -k_{\mathrm{L}} \frac{\partial}{\partial p_x} T^{\mathrm{L}}(p_{Mx}, p_y) + k_{\mathrm{S}} \frac{\partial}{\partial p_x} T^{\mathrm{S}}(p_{Mx}, p_y) \tag{43}$$

It is in present paper solved by the simple bisection.

4.2 Space discretization sensitivity for monophasic material

The method is first tested with constant unit thermal properties and monophasic material, i.e. $h_M = 0 J/(\mathrm{kg\,K})$. The computations are done with uniform domain discretizations of the type $N' \times 3$, with $N = 3 \times N - 4$, $N_\Gamma = 2 \times (N - 2) + 2$ and $N_\Omega = N - 2$, defined on a strip-shaped domains with longitudinal coordinates $p_x^- = 0\,\mathrm{m}$, $p_x^+ = 1\,\mathrm{m}$, and transversal coordinates $p_y^\pm = \pm 1.0\,\mathrm{m}/(N' - 1)$. The schematics of 21×3 discretization is shown in Figure 1. The steady-state solution is reached through a transient from the initial uniform temperature $T_0 = T_\Gamma^-$ and a jump of the boundary conditions at p_x^- from $T_\Gamma^- = 0\,\mathrm{K}$ to $T_\Gamma^+ = 1\,\mathrm{K}$ for $t > t_0$ and stopped through the steady state criterion (37). The steady-state criterion used in all calculations in this paper is $T_{\mathrm{ste}} = 10^{-7}\,\mathrm{K}$, the iteration criterion $T_{\mathrm{itr}} = 10^{-8}\,\mathrm{K}$ and the underrelaxation $\varepsilon = 0.02$. The steady state is reached with time-step $\Delta t = 10^{-5}\,\mathrm{s}$. The Péclet Pe and Stefan Ste numbers are, in the following steady-state examples of Section 4, defined as:

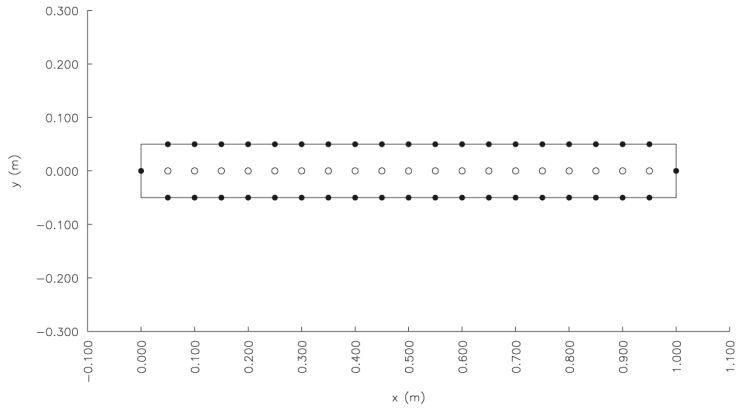

Figure 1.
Discretization schematics 21×3 for solving the quasi-one-dimensional convective diffusive problem

$$\mathrm{Ste} = \frac{c_{p0}\left(T_\Gamma^- - T_\Gamma^+\right)}{h_M} \tag{44}$$

$$\mathrm{Pe} = \frac{\rho_0 c_{p0} v_x \left(p_x^+ - p_x^-\right)}{k_0} \tag{45}$$

The maximum absolute temperature error $T_{\max}$ and the average absolute temperature error T_{avg} of the numerical solution at time t are defined as:

$$T_{\max} = \max|T(\mathbf{p}_n, t) - T_{\mathrm{ana}}(\mathbf{p}_n, t)|; \quad n = 1, 2, \ldots, N \tag{46}$$

$$T_{\mathrm{avg}} = \sum_{n=1}^{N} \frac{1}{N} |T(\mathbf{p}_n, t) - T_{\mathrm{ana}}(\mathbf{p}_n, t)|; \quad n = 1, 2, \ldots N \tag{47}$$

The maximum relative nodal temperature and interphase position errors are calculated from:

$$\gamma_{\max}(\%) = \left[\frac{\mathrm{sign}(\gamma(\mathbf{p}_n, t) - \gamma_{\mathrm{ana}}(\mathbf{p}_n, t))}{\gamma_{\mathrm{ana}}(\mathbf{p}_n, t)}\right] \max\left|\left(\frac{\gamma(\mathbf{p}_n, t) - \gamma_{\mathrm{ana}}(\mathbf{p}_n, t))}{\gamma_{\mathrm{ana}}(\mathbf{p}_n, t)}\right)\right| \times 100\%; \quad n = 1, 2, \ldots, N \tag{48}$$

where T and T_{ana} stand for numerical and analytical solution. γ stands for temperature or interphase position. The chosen error measures have been made compatible with the studies of Dalhuijsen and Segal (1986), Pardo and Weckman (1986) and Sarler and Kuhn (1998).

All RBFCM introduce some sort of a shape parameter c. The choice of the optimum value of this parameter is still an unresolved problem, and the optimum value is usually at the present state-of-the-art found using numerical experiments. The shape parameter c is considered constant and the same for all gridpoints. Since, the scaling cr_0 is used in present paper, the scaled shape parameter differs from subregion to subregion in general. Some authors (Mai-Dui and Tranh-Cong, 2001) claim that the shape parameter is related to the typical grid distance. Other researchers (Zhang *et al.*, 2000) did not find any relation, and claim simply that the optimum shape parameter is problem dependent. Very recently Wang and Liu (2002) analysed the extended multiquadric with the exponent being shape parameter as well. The authors concluded that by proper fixing of both parameters the solution becomes independent on the node density, node distribution and problem. Lee *et al.* (2003) found that the results are less sensitive to the choice of the free parameter in the local collocation method as in the global ones. Our investigation in Table I shows that the results are improving with the growth of the free parameter from 1 to 32 for both fine grids used 101×3, 201×3, and are optimal at 16 for grid 51×3.

C	Discretisation	cr_0	T_{avg}(K)	T_{max}(K)
1.0	51×3	0.04	0.765300	0.98220000
1.0	101×3	0.02	0.880900	0.99970000
1.0	201×3	0.01	0.920500	0.99990000
2.0	51×3	0.08	0.247900	0.41920000
2.0	101×3	0.04	0.586300	0.82590000
2.0	201×3	0.02	0.823500	0.99450000
4.0	51×3	0.16	0.021349	0.03808800
4.0	101×3	0.08	0.084033	0.14730000
4.0	201×3	0.04	0.277900	0.45900000
8.0	51×3	0.32	0.001278	0.00321820
8.0	101×3	0.16	0.005665	0.01004100
8.0	201×3	0.08	0.023036	0.04078300
16.0	51×3	0.64	0.000633	0.00475410
16.0	101×3	0.32	0.000326	0.00076631
16.0	201×3	0.16	0.001448	0.00256500
32.0	51×3	1.28	0.000640	0.00485680
32.0	101×3	0.64	0.000155	0.00117190
32.0	201×3	0.32	0.000084	0.00017138

Table I. Monophasic material. Influence of the multiquadric shape parameter on solution $Pe = 20.0$ at three discretizations

It is also evident from Table I that the method converges with finer space discretization. From Table II and from Figure 2(a)-(c) one can conclude that the error grows with higher Péclet number.

4.3 Space discretization sensitivity for phase-change material

The method is tested next with the constant unit phase-change material. The isothermal melting temperature $T_M = 0.950\,\mathrm{K}$ is, in the calculations, approximated by a narrow temperature range $T_S = 0.945\,\mathrm{K}$, $T_L = 0.955\,\mathrm{K}$ and linear variation of the liquid fraction over this temperature interval. The same steady state approaching transient is made as in the previous monophasic example. Figure 3 shows the sensitivity of the method with respect to Péclet number, and Figure 4 shows the sensitivity of the method with respect to Stefan number. Related numerical data are given in Tables III and IV. The fact that the temperature accuracy degrades with lower Stefan numbers and higher Péclet numbers is a common expected feature of all one-domain methods. All interphase position errors have been evaluated at $p_y = 0\,\mathrm{m}$ in this paper. The position of the interphase boundary is consistently underpredicted in cases with constant material properties of phases – a fact that compares well with the studies by Pardo and Weckman (1986) and Šarler and Kuhn (1998).

Pe	T_{avg}(K)	T_{max}(K)
0	0.000143	0.000224
10	0.000054	0.000202
20	0.000155	0.001172
30	0.000245	0.002734
40	0.000329	0.004864
50	0.000412	0.007854

Table II. Monophasic material. Sensitivity of the results with respect to Péclet number at discretisation 101×3 and the scaled multiquadrics free parameter $c \cdot r_0 = 0.64\,\mathrm{m}$

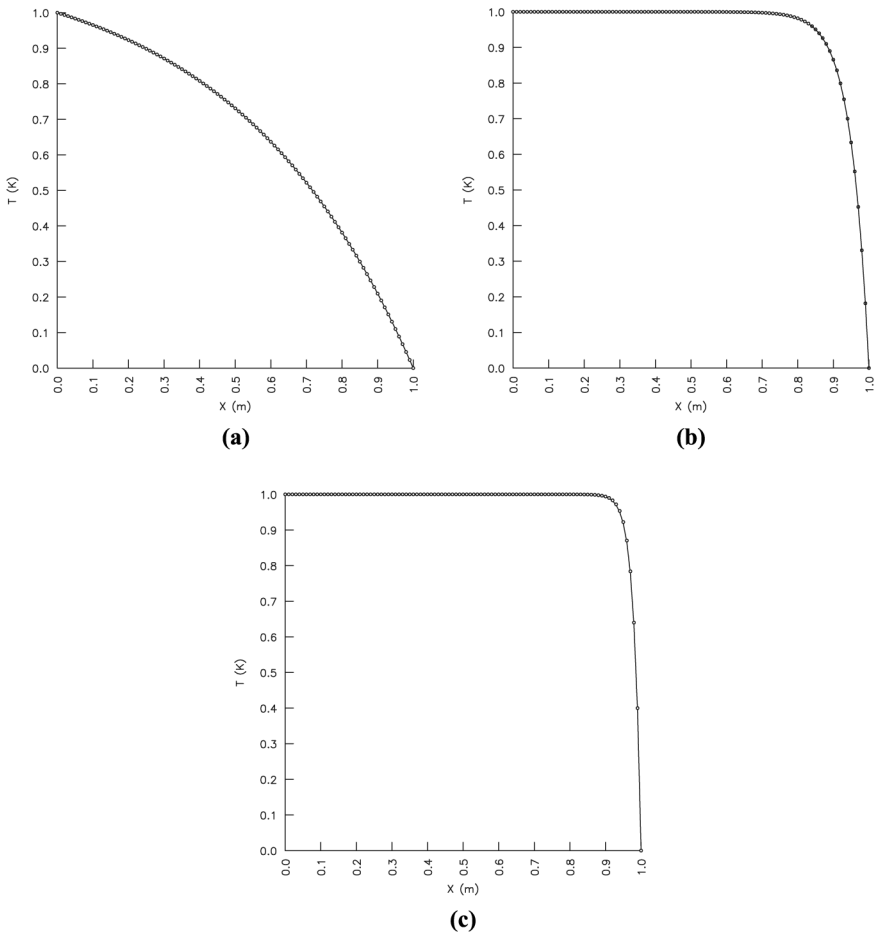

Figure 2.
Monophasic material

Notes: Comparison of the calculated temperatures ○ in the central nodes at p_y = 0m with the analytical solution -. Discretisation 101×3. (a) Pe = 2, (b) Pe = 20, (c) Pe = 50. The scaled multiquadrics free parameter is set to cr_0 = 0.64m

Table V shows a comparison of the maximum relative temperature errors of our method (LRBFCM) with the reference FEM calculations (Pardo and Weckman, 1986) and dual reciprocity boundary element method (DRBEM) calculations (Šarler and Kuhn, 1998) (Figures 5 and 6)) Table VI. The disrcetisation in FEM, that corresponds to LRBFCM discretisation $N' \times 3$ is equal to $N' - 1$ isoparametric hexahedral linear finite elements. The related discretisation in DRBEM is equal to $2 \times (N' - 1) + 4$ constant boundary elements and $N' - 1$ domain points. The present method gives comparable results in terms of overall temperature accuracy and interphase boundary position error at the compared node densities. The convergence of our method in this comparison exercise is shown in Figure 7(a)-(c).

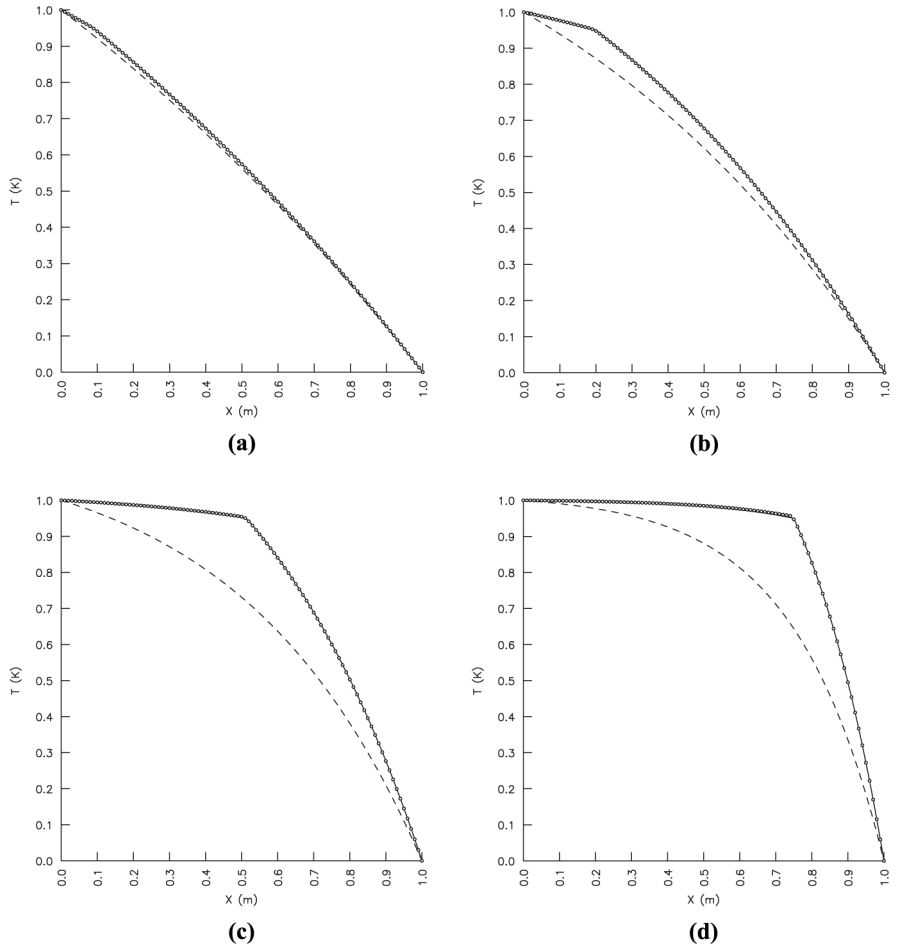

Notes: Comparison of calculated temperatures ○ in the central nodes p_y = 0m with analytical solution for different Péclet numbers. Line - - denotes analytical solution with Ste = ∞. Discretisation 101×3. Ste = 2.0. (a) Pe = 0.5, (b) Pe = 1.0, (c) Pe = 2.0 and (d) Pe = 4.0

Figure 3.

4.4 Space discretization sensitivity for different material properties of the phases

The thermal conductivities of the solid and liquid phases at the melting point or in the phase-change interval usually do not differ by more than 100 per cent in pure metals or alloys. Similarly, the related alloy specific heats do not differ by more than 25 per cent (Brandes and Brook, 1992). In the present study of the influence of the different material properties on the results of the present numerical method, the cases with three times greater or lower thermal conductivity and cases with two times lower or greater specific heat have been recalculated, which most probably covers all realistic situations. The results of these calculations are shown in Figure 6(a)-(d) and Table VII.

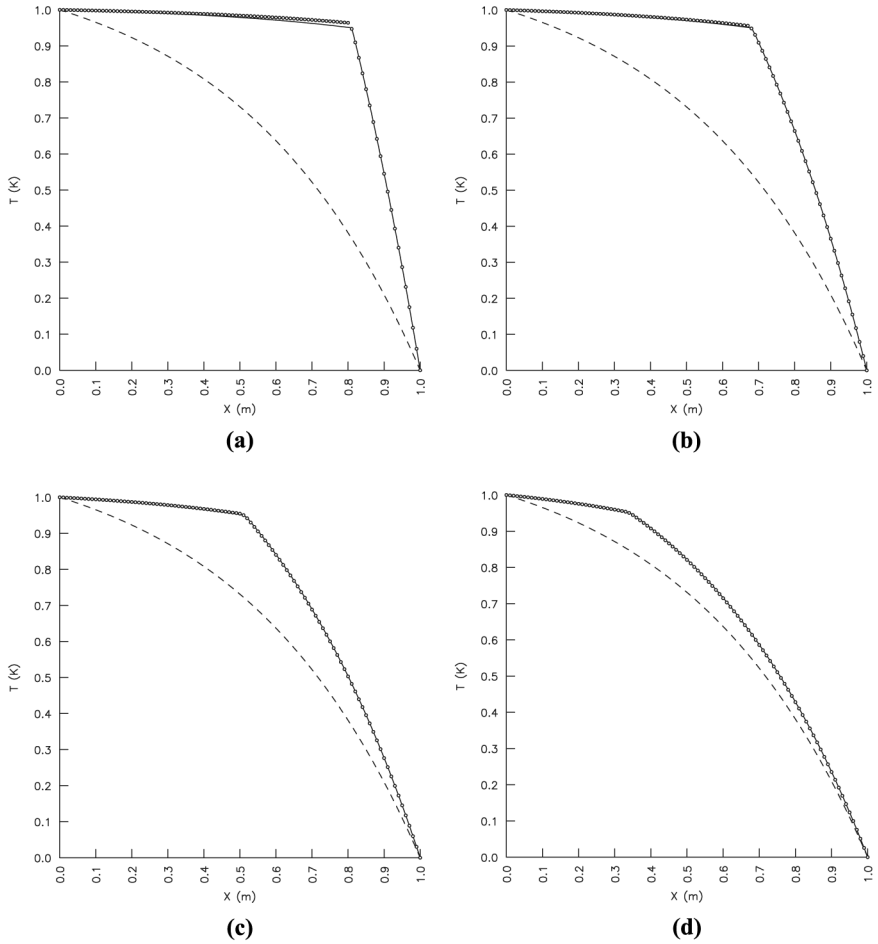

Figure 4.

Notes: Comparison of calculated temperatures ○ in the central nodes p_y = 0m with analytical solution – for different Stefan numbers. Line - - denotes analytical solution with Ste = ∞. Discretisation 101×3. Pe = 2.0. (a) Ste = 0.5, (b) Ste = 1.0, (c) Ste = 2.0 and (d) Ste = 4.0

Table III.
Sensitivity of the results with respect to Péclet number at discretisation 101 × 3, Ste = 2.0

Pe	T_{avg}(K)	T_{max}(K)	p_{Mx}(m)	$P_{err\ x}$(m)
0.5	0.000206	0.000635	0.089150	− 0.000329
1.0	0.000977	0.002406	0.200251	− 0.000161
2.0	0.000908	0.002528	0.513854	− 0.003082
4.0	0.001064	0.004949	0.749926	− 0.000662

The accuracy of the results does not principally differ from the accuracy of the cases with constant material properties.

4.5 Direct-chill casting problem

Direct-chill (DC) casting is currently the most common (Altenpohl, 1998) semi-continuous casting practice in production of aluminum alloys. The process involves molten metal being feed through a bottomless water-cooled mould where it is sufficiently solidified around the outer surface that it takes the shape of the mould and acquires sufficient mechanical strength to contain the molten core at the center. As the strand emerges from the mould, water impinges directly from the mould onto the surface (DC), falls over the cast surface and completes the solidification. This section elaborates the solution of a simplified model of the DC casting process by the developed LRBFCM in two dimensions (Figures 8 and 9). The steady state solution is shown in this paper, approached by a false transient calculation using a fixed time-step of 0.5 s. The enthalpy reference temperature T_{ref} has been set to 0 K. The following simplified DC casting case is considered. The computational domain is a rectangle (coordinates p_x, p_y) $-1.25\,\text{m} \le p_y \le 0\,\text{m}$, $0\,\text{m} \le p_x \le 0.25\,\text{m}$. The boundary conditions on the top at $p_y = 0\,\text{m}$ are of the Dirichlet type with $T_\Gamma^{\text{D}} = 980\,\text{K}$, and the boundary conditions at the bottom at $p_y = -1.25\,\text{m}$ are of the Neumann type with $F_\Gamma^{\text{N}} = 0\,\text{W/m}^2$. The boundary conditions at the outer surface are of the Robin type with $T_{\Gamma\text{ref}}^{\text{R}} = 298\,\text{K}$. The heat transfer coefficients between $0\,\text{m} \le p_y \le -0.01\,\text{m}$, $-0.0\,\text{m} \le p_y \le -0.06\,\text{m}$, $-0.06\,\text{m} \le p_y \le -0.1\,\text{m}$, and $-0.1\,\text{m} \le p_y \le -1.25\,\text{m}$, are $T_\Gamma^{\text{R}} = 0\,\text{W/m}^2\text{K}$, $T_\Gamma^{\text{R}} = 3,000\,\text{W/m}^2\text{K}$, $T_\Gamma^{\text{R}} = 150\,\text{W/m}^2\text{K}$, and $T_\Gamma^{\text{R}} = 4,000\,\text{W/m}^2\text{K}$,, respectively. Material properties correspond to a simplified Al4.5%Cu alloy as already used in Šarler and Mencinger (1999) and Šarler *et al.* (2005): $\rho_{\text{S}} = \rho_{\text{L}} = 2,982\,\text{kg/m}^3$, $k_{\text{S}} = 120.7\,\text{W/m K}$, $k_{\text{L}} = 57.3\,\text{W/m K}$, $k = f_{\text{S}}^{\text{V}} k_{\text{S}} + f_{\text{L}}^{\text{V}} k_{\text{L}}$, $c_{\text{S}} = 1,032\,\text{W/m K}$, $c_{\text{L}} = 1,179\,\text{W/m K}$, $h_M = 348.2\,\text{kJ/kg K}$, $T_{\text{S}} = 775\,\text{K}$, $T_{\text{L}} = 911\,\text{K}$. The liquid fraction increases linearly between T_{S} and T_{L}. The initial conditions are described by a linear variation of the temperature with the p_x coordinate from 298 K

Ste	T_{avg}(K)	$T_{\max}$(K)	p_{Mx}(m)	$P_{\text{err } x}$ (m)
0.5	0.003857	0.012703	0.810560	−0.000543
1.0	0.001407	0.004705	0.671921	−0.001538
2.0	0.000908	0.002528	0.513854	−0.003082
4.0	0.000742	0.001291	0.335296	−0.002565

Table IV. Sensitivity of the results with respect to Stefan number at discretisation 101×3, Pe = 2.0

Grid	$21 \times 3\,(c \cdot r_0 = 1.6)$	$41 \times 3\,(c \cdot r_0 = 0.8)$	$81 \times 3\,(c \cdot r_0 = 0.4)$
LRBFCM $T_{\max}$ (per cent)	2.57	1.24	0.41
DRBEM $T_{\max}$ (per cent)	1.21	0.81	0.41
FEM $T_{\max}$ (per cent)	2.15	1.06	0.46

Note: Comparison of the maximum nodal temperature error of the present method (LRBFCM) with results of the FEM by Pardo and Weckman (1996) and the dual reciprocity boundary element method by Šarler and Kuhn (1998). Pe = 2.0 1/Ste = 0.7

Table V.

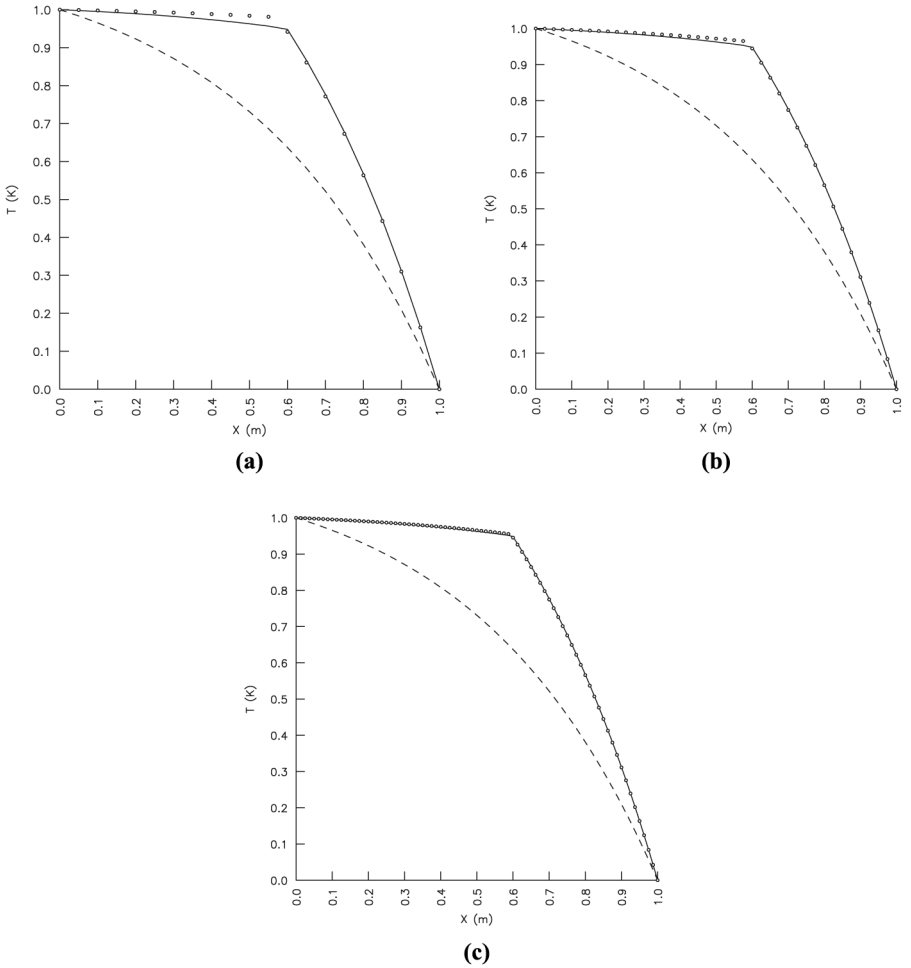

Notes: Comparison of calculated temperatures ○ in the central nodes p_y = 0m with analytical solution – for test case from Pardo and Weckman (1996). Line - - denotes analytical solution with Ste = ∞. Pe = 2.0. 1/Ste = 0.7. Discretisation (a) 21×3, (b) 41×3, and (c) 81×3

Figure 5.

at the bottom to 980 K at the top of the cylinder. The uniform casting velocity is $v_{Sy} = v_{Ly} = -0.000633\,\mathrm{m/s}$, $v_{Sx} = v_{Lx} = 0\,\mathrm{m/s}$. The solution has been obtained on an equidistant 27×127 node arrangement as well as randomly displaced node arrangement. A schematic of the uniform node arrangement 27×127 is shown in Figure 7 (left). A non-uniform node arrangement is generated from the uniform node arrangement through transformation:

$$p_{n\varsigma(\mathrm{non-uniform})} = p_{n\varsigma(\mathrm{uniform})} + c_{\mathrm{random}}\,\delta r_{\min}\,p_{n\varsigma(\mathrm{uniform})}; \quad \varsigma = x, y \tag{49}$$

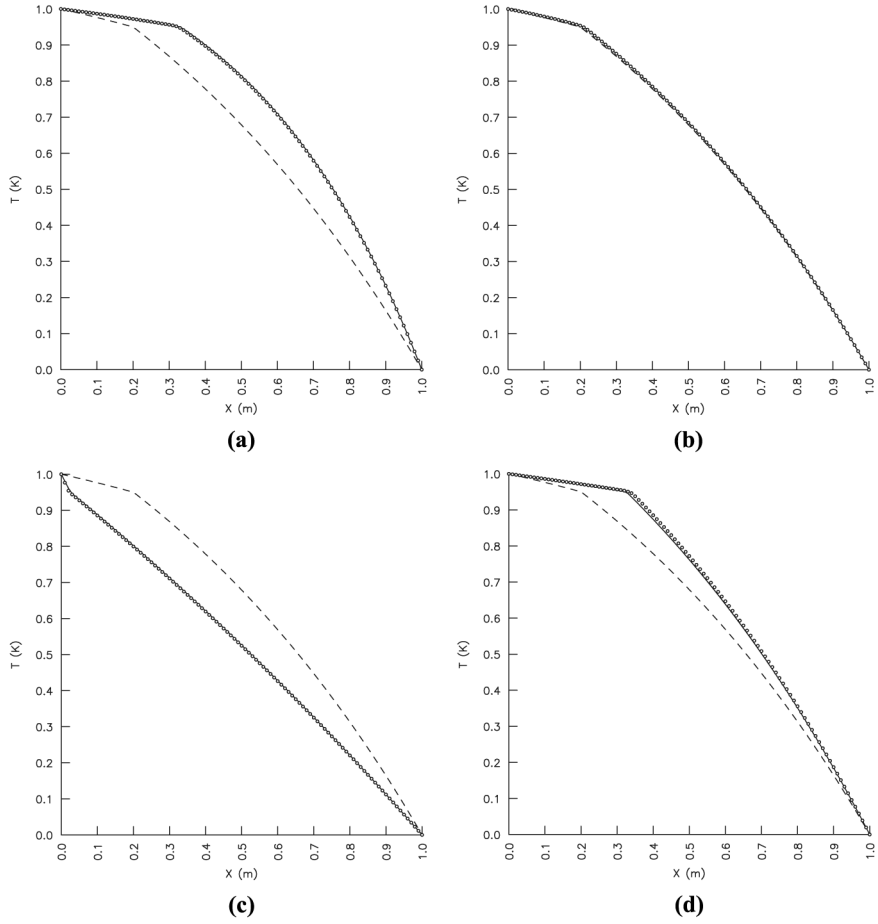

Notes: Comparison of calculated temperatures O in the central nodes p_y =0m with analytical solution –. Line - - denotes analytical solution with unit material properties. Discretisation 101×3. Pe = 1.0. Ste = 2.0. (a) c_{pS0} = 2.0J/kgK, (b) c_{pL0} = 2.0J/kgK, (c) k_{S0} = 3.0W/mK, and (d) k_{L0} = 3.0 W/mK

Figure 6.

Grid	$21 \times 3\,(c \cdot r_0 = 1.6)$	$41 \times 3\,(c \cdot r_0 = 0.8)$	$81 \times 3\,(c \cdot r_0 = 0.4)$
LRBFCM $p_{\max\ x}$(per cent)	−1.68	−1.33	−0.94
DRBEM $p_{\max\ x}$(per cent)	−1.51	−0.77	−0.46
FEM $p_{\max\ x}$(per cent)	−1.62	−0.82	−0.48

Note: Comparison of the interphase position error of the present method with results of the FEM by Pardo and Weckman (1986) and the dual reciprocity boundary element method (DRBEM) by Šarler and Kuhn (1998). Pe = 2.0, 1/Ste = 0.7, p_{Mx} = 0.598739 m

Table VI.

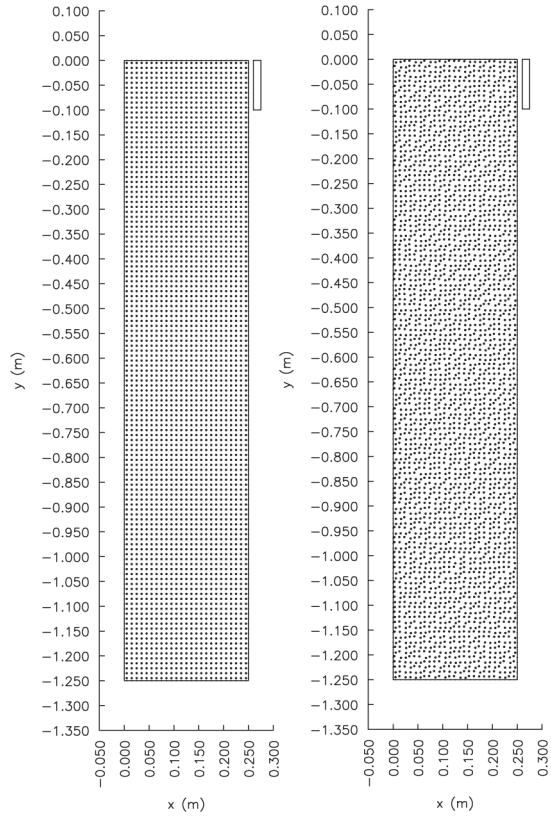

Figure 7.
Left: 27×127 uniform node arrangement. Right: 27×127 non-uniform randomly displaced node arrangement. The upper right rectangle schematically represents the mold

Table VII.
Sensitivity of the results with respect to different material properties of the phases. Discretisation 101×3, Pe = 1.0, Ste = 2.0

c_{pS0}	c_{pL0}	k_{S0}	k_{L0}	T_{avg} (K)	T_{max} (K)	P_{Mx} (m)	$p_{err\ x}$ (m)
1.0	1.0	1.0	1.0	0.000978	0.002406	0.200251	−0.000161
2.0	1.0	1.0	1.0	0.001478	0.003105	0.331708	−0.001201
1.0	2.0	1.0	1.0	0.000292	0.001009	0.210841	−0.000516
1.0	1.0	3.0	1.0	0.001430	0.006821	0.025634	0.001914
1.0	1.0	1.0	3.0	0.005002	0.012371	0.325451	−0.003810

where c_{random} represents a random number $-1 \leq c_{random} \leq +1$, δ represents a displacement factor (in this work fixed to 0.25), and r_{min} the minimum distance between the two nodes in the uniform node arrangement. Only domain nodes have been subject to this transformation (Figure 7 (right)). In the uniform-grid and non-uniform grid calculations the shape parameter $c = 16.0$ is used. The uniform grid has been calculated with a five-noded support and the non-uniform grid with the seven-noded support. The computational effort is approximately two, five times greater as with the FVM method. Figure 10 shows comparison between present results

Notes: Dashed curve – surface temperature, dotted curve – mid-radius temperature, and dot-dashed curve – centerline temperature

Figure 8.
Absolute difference between the LRBFCM solutions calculated in uniform and non-uniform node arrangements

and FVM. There is practically no visual difference. Figure 11 shows the absolute error between the two solutions. A similar comparison has been performed also with the DAM and FVM in Šarler *et al.* (2005) with the maximum difference between DAM and FVM about 4 times bigger as in the present method. For the solution of the presented problem with DAM (Šarler *et al.*, 2005), we need six polynomial basis and at least nine neighbouring points in support which makes this meshless approach also less efficient as the present one.

5. Conclusions

This paper represents a new (very) simple mesh-free formulation for solving a wide range of convection-diffusion problems with phase change. The time marching is performed in a simple explicit way. The governing equation is solved in its strong form. No polygonisation and integrations are needed. The developed method is almost independent of the problem dimension. The complicated geometry can easily be coped with. The method appears efficient, because it does not require a solution of a large system of equations like the original Kansa method. Instead, small systems of linear equations have to be solved in each time-step for each node and associated domain of influence, probably representing the most natural and automatic domain decomposition. This feature of the developed method represents its principal difference from the other related local approaches, where the resultant matrix is large and sparse (Lee *et al.*, 2003; Shu *et al.*, 2003; Tolstykh and Shirobokov, 2005). The method is simple to learn and simple to code. The method can cope with very large

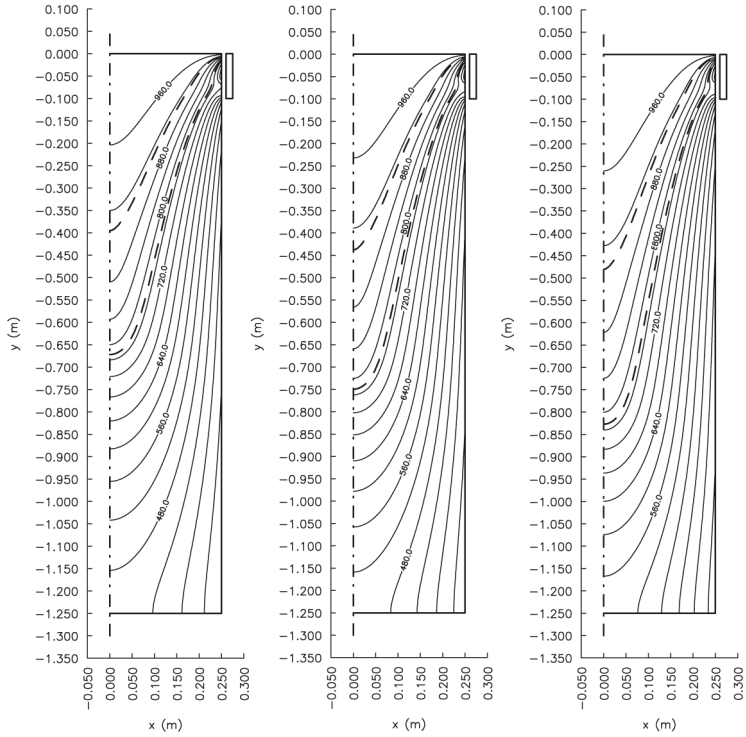

Notes: Temperature field in the slab. Solidus and liquidus isotherms are dashed. Central figure – normal casting velocity, left figure – reduced casting velocity for 10%, right figure – enhanced casting velocity for 10%

Figure 9.
LRBFCM results

problems since the computational effort grows approximately linear with the number of the nodes. The developments in this paper can be straightforwardly extended to tackle other types of PDEs. When compared with other mesh-reduction or -free methods used in the context of the represented industrial example, one can conclude: The method can cope with physically more involved situations than the front tracking BEM (Fic *et al.*, 2000), where the calculations are limited to a uniform velocity field, constant material properties of the phases, and isothermal phase-change. When compared to DRBEM (Šarler and Kuhn, 1998), the method does not need any integrations and boundary polygonisation. The method appears much more efficient as the RBFCM (Kovačević *et al.*, 2003), because it does not require a solution of the large systems of equations. Instead, small (5×5 and 7×7 used in present paper) systems of linear equations have to be solved in each time-step for each node. Our ongoing research is focused on the extension of the method to implicit time-marching which might overcome the inherent stability problem of the explicit approach and the use of the method in coupled transport phenomena context.

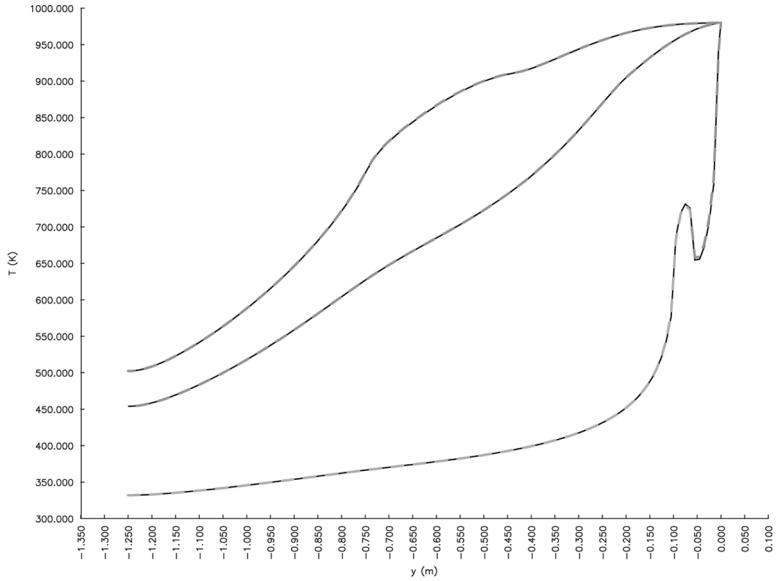

Notes: Solid curve: FVM, bold dashed curve: LRBFCM. Upper curve – centerline temperature, center curve – mid-radius temperature, and lower curve – surface temperature

Figure 10.
Calculated temperature distribution in the slab. 27×127 node arrangement

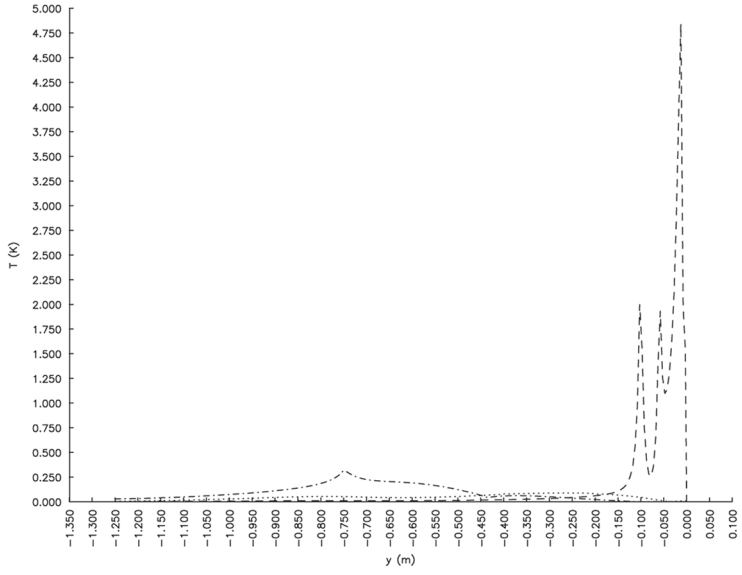

Notes: Dashed curve – surface temperature, dotted curve – mid-radius temperature, and dot-dashed curve – centerline temperature

Figure 11.
Absolute difference between the FVM and the LRBFCM solutions

References

Altenpohl, D.G. (1998), *Aluminum: Technology, Applications, and Environment: A Profile of a Modern Metal*, Aluminium Association & TMS, Warrendale.

Atluri, S.N. (2004), *The Meshless Method for Domain and BIE Discretisations*, Tech Science Press, Forsyth, GA.

Atluri, S.N. and Shen, S. (2002), *The Meshless Method*, Tech Science Press, Forsyth, GA.

Bennon, W.D. and Incropera, F.P. (1987), "A continuum model for momentum, heat and species transport in binary solid-liquid phase change systems – I. Formulation", *International Journal of Heat and Mass Transfer*, Vol. 30, pp. 2161-70.

Brandes, E.A. and Brook, G.B. (1992), *Smithells Metals Reference Book*, 7th ed., Butterworth-Heinemenn, Oxford.

Buhmann, M.D. (2003), *Radial Basis Function: Theory and Implementations*, Cambridge University Press, Cambridge.

Chen, W. (2002), "New RBF collocation schemes and kernel RBFs with applications", *Lecture Notes in Computational Science and Engineering*, Vol. 26, pp. 75-86.

Dalhuijsen, A.J. and Segal, A. (1986), "Comparison of finite element techniques for solidification problems", *International Journal for Numerical Methods in Engineering*, Vol. 29, pp. 1807-29.

Fasshauer, G.E. (1997), "Solving partial differential equations by collocation with radial basis functions", in Mehaute, A.L., Rabut, C. and Schumaker, L.L. (Eds), *Surface Fitting and Multiresolution Methods*, Vanderbilt University Press, Nashville, TN, pp. 131-8.

Fic, A., Nowak, A.J. and Białecki, R. (2000), "Heat transfer analysis of the continuous casting process by the front tracking BEM", *Engineering Analysis with Boundary Elements*, Vol. 24, pp. 215-23.

Kansa, E.J. (1990), "Multiquadrics – a scattered data approximation scheme with applications to computational fluid dynamics-II. Solutions to parabolic, hyperbolic and elliptic partial differential equations", *Computers and Mathematics with Application*, Vol. 19, pp. 147-61.

Kovačević, I., Poredoš, A. and Šarler, B. (2003), "Solving the Stefan problem by the RBFCM", *Numerical Heat Transfer, Part B: Fundamentals*, Vol. 44, pp. 575-99.

Lee, C.K., Liu, X. and Fan, S.C. (2003), "Local muliquadric approximation for solving boundary value problems", *Computational Mechanics*, Vol. 30, pp. 395-409.

Liu, G.R. (2003), *Mesh Free Methods*, CRC Press, Boca Raton, FL.

Mai-Duy, N. and Tran-Cong, T. (2001), "Numerical solution of differential equations using multiquadrics radial basis function networks", *International Journal for Numerical Methods in Engineering*, Vol. 23, pp. 1807-29.

Mai-Duy, N. and Tran-Cong, T. (2002), "Mesh-free radial basis function network methods with domain decomposition for approximation of functions and numerical solution of Poisson's equations", *Engineering Analysis with Boundary Elements*, Vol. 26, pp. 133-56.

Mai-Duy, N. and Tran-Cong, T. (2003), "Indirect RBFN method with thin plate splines for numerical solution of differential equations", *Computer Modeling in Engineering & Sciences*, Vol. 4, pp. 85-102.

Nayroles, B., Touzot, G. and Villon, P. (1991), "The diffuse approximation", *C.R. Acad. Sci. Paris*, Vol. 313-II, pp. 293-6.

Özisik, M.N. (1994), *Finite Difference Methods in Heat Transfer*, CRC Press, Boca Raton, FL.

Pardo, E. and Weckman, D.C. (1986), "A fixed grid finite element technique for modelling phase change in steady-state conduction-advection problems", *International Journal for Numerical Methods in Engineering*, Vol. 23, pp. 1807-29.

Perko, J. (2005), "Modelling of transport phenomena by the diffuse approximate method", doctoral dissertation, School of Applied Sciences, Nova Gorica Polytechnic, Nova Gorica.

Power, H. and Barraco, W.A. (2002), "Comparison analysis between unsymmetric and symmetric RBFCMs for the numerical solution of PDE's", *Computers and Mathematics with Applications*, Vol. 43, pp. 551-83.

Sadat, H. and Prax, C. (1996), "Application of the diffuse approximation for solving fluid flow and heat transfer problems", *International Journal of Heat and Mass Transfer*, Vol. 39, pp. 214-8.

Šarler, B. (2004), "Meshless methods", in Nowak, A.J. (Ed.), *Advanced Numerical Methods in Heat Transfer*, Chapter 9, Silesian Technical University Press, Gliwice, pp. 225-47.

Šarler, B. (2005), "A radial basis function collocation approach in computational fluid dynamics", *Computer Modeling in Engineering & Sciences*, Vol. 7, pp. 185-93.

Šarler, B. and Kuhn, G. (1998), "Dual reciprocity boundary element method for convective-diffusive solid-liquid phase change problems, Part 2. Numerical examples", *Engineering Analysis with Boundary Elements*, Vol. 21, pp. 65-79.

Šarler, B. and Mencinger, J. (1999), "Solution of temperature field in DC cast aluminium alloy billet by the dual reciprocity boundary element method", *International Journal of Numerical Methods in Heat & Fluid Flow*, Vol. 9, pp. 267-97.

Šarler, B., Perko, J. and Chen, C.S. (2004), "Radial basis function collocation method solution of natural convection in porous media", *International Journal of Numerical Methods for Heat & Fluid Flow*, Vol. 14, pp. 187-212.

Šarler, B. and Vertnik, R. (2005), "Meshfree explicit radial basis function collocation method for diffusion problems", *Computers and Mathematics with Applications*(in press).

Šarler, B., Vertnik, R. and Perko, J. (2005), "Application of diffuse approximate method in convective-diffusive solidification problems", *Computers, Materials, Continua*, Vol. 2, pp. 77-83.

Shu, C., Ding, H. and Yeo, K.S. (2003), "Local radial basis function-based differential quadrature method and its application to solve two-dimensional incompressible Navier-Stokes equations", *Computer Methods in Applied Mechanics and Engineering*, Vol. 192, pp. 941-54.

Tolstykh, A.I. and Shirobokov, D.A. (2005), "Using radial basis functions in a 'finite difference mode'", *Computer Modeling in Engineering & Sciences*, Vol. 7, pp. 207-22.

Versteeg, H.K. and Malalasekera, W. (1995), *An Introduction to Computational Fluid Dynamics: The Finite Volume Method*, Longman Scientific & Technical, Harlow.

Vertnik, R., Perko, J. and Šarler, B. (2004), "Solution of temperature field in DC cast aluminium alloy billet by the diffuse approximate method", *Materials and Technology*, Vol. 38, pp. 257-61.

Voller, V.R., Swaminathan, S. and Thomas, B.G. (1990), "Fixed-grid techniques for phase-change problems – a review", *International Journal of Numerical Methods in Engineering*, Vol. 30, pp. 875-98.

Wang, J.G. and Liu, G.R. (2002), "On the optimal shape parameter of radal basis functions used for 2-D mesheless method", *Computer Methods in Applied Mechanics and Engineering*, Vol. 26, pp. 2611-30.

Wrobel, L.C. (2001), *The Boundary Element Method –Volume 1: Applications in Thermofluids and Acoustics*, Willey, New York, NY.

Zhang, X., Song, K.Z., Lu, M.W. and Liu, X. (2000), "Meshless methods based on collocation with radial basis functions", *Computational Mechanics*, Vol. 26, pp. 333-43.

Zienkiewicz, O.C. and Taylor, R.L. (2000), *The Finite Element Method, Volume 1: The Basis*, Vol. 1, Butterworth-Heinemann, Oxford.

Further reading

Šarler, B., Kovačević, I. and Chen, C.S. (2004), "A mesh-free solution of temperature in direct-chill cast slabs and billets", in Mammoli, A.A. and Brebbia, C.A. (Eds), *Moving Boundaries VII*, WIT Press, Southampton, pp. 271-80.

Tolstykh, A.I. and Shirobokov, D.A. (2003), "On using radial basis functions in a 'finite difference mode' with applications to elasticity problems", *Computational Mechanics*, Vol. 33, pp. 68-79.

Venneker, B.C.H. and Katgerman, L. (2002), "Modelling issues in macrosegregation predictions in direct-chill casting", *Journal of Light Metals*, Vol. 2, pp. 149-59.

Zerroukat, M., Power, H. and Chen, C.S. (1998), "A numerical method for heat transfer problems using collocation and radial basis functions", *International Journal for Numerical Methods in Engineering*, Vol. 42, pp. 1263-78.